Co-Crystallization with Conformation-Specific Designed Ankyrin Repeat Proteins Explains the Conformational Flexibility of BCL-W

Johannes Schilling [1,†], Jendrik Schöppe [1,†], Evelyn Sauer [2] and Andreas Plückthun [1]

*1 - **Biochemisches Institut,** Universität Zürich, Winterthurerstrasse 190, CH-8057 Zürich, Switzerland*
*2 - **Biozentrum,** Universität Basel, Klingelbergstrasse 50/70, CH-4056 Basel, Switzerland*

Correspondence to Andreas Plückthun: *plueckthun@bioc.uzh.ch*
http://dx.doi.org/10.1016/j.jmb.2014.04.010
Edited by Y. Shi

Abstract

BCL-W is a member of the BCL-2 family of anti-apoptotic proteins. A key event in the regulation of apoptosis is the heterodimerization between anti-apoptotic and pro-apoptotic family members, which involves a conserved surface-exposed groove on the anti-apoptotic proteins. Crystal structures of the ligand binding-competent conformation exist for all anti-apoptotic family members, with the exception of BCL-W, due to the flexibility of the BCL-W groove region. Existing structures had suggested major deviations of the BCL-W groove region from the otherwise structurally highly related remaining anti-apoptotic family members. To capture its ligand binding-competent conformation by counteracting the conformational flexibility of the BCL-W groove, we had selected high-affinity groove-binding designed ankyrin repeat proteins (DARPins) using ribosome display. We now determined two high-resolution crystal structures of human BCL-W in complex with different DARPins at resolutions 1.5 and 1.85 Å, in which the structure of BCL-W is virtually identical, and BCL-W adopts a conformation extremely similar to the ligand-free conformation of its closest relative BCL-XL in both structures. However, distinct differences to all previous BCL-W structures are evident, notably in the ligand-binding region. We provide the first structural explanation for the conformational flexibility of the BCL-W groove region in comparison to other BCL-2 family members. Due to the importance of the anti-apoptotic BCL-2 family as drug targets, the presented crystal structure of ligand binding-competent BCL-W may serve as a valuable basis for structure-based drug design in the future and provides a missing piece for the structural characterization of this protein family.

Introduction

Apoptosis is a crucial part of development and tissue turnover. It is conserved between organisms as distantly related as worms and man. The perturbation of its regulation is critically involved in diseases, both when apoptosis becomes overly active (e.g., autoimmune disorders) and when inappropriately turned off (e.g., cancer) [1–5].

The BCL-2 family of proteins are important regulators of programmed cell death and their balanced interplay is thus tightly regulated [6–9]. They share one or more homologous sequence regions, the so-called BCL-2 homology regions (BH1, BH2, BH3 and BH4), which are required for their function [6]. The family can be divided into three subfamilies: (i) anti-apoptotic members including BCL-2, BCL-XL, BCL-W and MCL-1, which contain all four BH regions; (ii) pro-apoptotic members, which possess only BH1, BH2 and BH3 regions and act as death effectors (e.g., BAX and BAK); and finally (iii) the pro-apoptotic BH3-only members (e.g. BIM, BAD, BID, BIK), which link upstream death stimuli, such as the stimulation of the tumor necrosis factor family of receptors or stress signals mediated by p53, to the regulation of the multi-BH region members of the family [10].

Survival or cell death in response to these signals is determined by the ratio of pro-apoptotic *versus* anti-apoptotic BCL-2 family members, and alterations in this ratio often result in disease susceptibility. In many cancers, for example, enhanced expression of anti-apoptotic members is found. BCL-2 is up-regulated in follicular lymphoma, leukemia, breast and lung cancers [11–14]; BCL-XL, in

myeloid and T-cell leukemia and in liver cancer [12]; BCL-W, in colorectal carcinoma [15]; and MCL-1, in ovarian carcinoma [16] and multiple myelomas [17]. Thus, anti-apoptotic BCL-2 family members have recently attracted significant attention as therapeutic targets [18].

The first published structure of a BCL-2 family member was that of human BCL-XL determined by X-ray crystallography and NMR spectroscopy more than 15 years ago [19] (Fig. 1a). Structures of other family members followed (BCL-2 [20], BCL-W [21,22] and MCL-1 [23]). They revealed that the overall structures of all BCL-2 family members were very similar to each other.

A structure-based sequence alignment of the mentioned anti-apoptotic BCL-2 family is shown in Fig. S1. The structure of the biologically active form of BCL-XL lacking the C-terminal transmembrane region (BCL-XLΔC24) can serve as a representative to describe the structure of anti-apoptotic BCL-2 family members. The fold consists of eight α-helices connected by loops of various lengths (Fig. 1a). The two central helices α5 and α6 form the core of the protein and are predominantly hydrophobic. They are flanked on one side by helices α3 and α4 and on the other side by helices α1 and α2. A key feature of anti-apoptotic BCL-2 family members is their conserved surface-exposed hydrophobic groove formed by four of these amphipathic helices (α3-α4 and α5-α6). The BH3 (end of α2) and BH1 (end of α4, α4-α5 hinge and beginning of α5) regions are highly conserved among BCL-2 family members and define, together with the α2-α3 hinge, which is conserved between BCL-XL and BCL-W, the entrance of the elongated hydrophobic groove (cf. Fig. S1). The end of the groove is defined by the α-hairpin formed by α3 and α4.

This hydrophobic groove was postulated, and confirmed through interaction studies and structure determination of the complexes, to be the interaction site with the pro-apoptotic members of the BCL-2 family [24]. Through this interaction, the anti-apoptotic BCL-2 family members titrate out BH3-only proteins and thus prevent them from driving apoptosis forward [1,6,7,25].

Therefore, small molecules or peptides [26–35] and proteins [36] used as BH3-only mimetics have recently been developed. Thus, for further progress in this field, accurate structural data of the groove region and the understanding of the structural mechanism governing the function of the anti-apoptotic BCL-2 family members have become indispensable.

However, available structural information for BCL-W is much more limited than for all other anti-apoptotic BCL-2 family members. It is unique among the anti-apoptotic BCL-2 family members in that it possesses an additional C-terminal helix (α9) preceding the transmembrane helix. While several crystal structures exist for both the ligand-bound state (BH3-only peptide-bound) and the ligand-free state of BCL-2, BCL-XL and MCL-1, no ligand-bound structure has been determined for BCL-W.

The first structural information of ligand-free BCL-W became available in 2003 with two published NMR structures (BCL-WΔC22 [21] and BCL-WΔC10 [22]) (Fig. 1b). These structures showed that BCL-W possesses an overall fold similar to the other anti-apoptotic BCL-2 family members. Surprisingly, however, the additional C-terminal helix (α9) bound into the surface groove of BCL-W. Helix α9 was significantly more mobile than the other α-helices of BCL-W, suggesting a low-affinity interaction between α9 and the groove, and it was postulated that binding of pro-apoptotic BH3-only proteins to BCL-W required the displacement of this helix [21]. Significant deviations existed between the two NMR structures of BCL-W on the one hand (Fig. 1b) and the BCL-XL structure (Fig. 1a and d) on the other hand in the regions of the groove, the α2-α3 hinge and α4-α5 hinge region.

Almost a decade passed until recently the first X-ray structure of a further truncated version of BCL-W (BCL-WΔC29) [37] was determined, showing a large displacement of the important groove formed by α3-α4 due to domain swapping (Fig. 1c). Thus, instead of clarifying the structural situation around the groove and hinge regions, this first crystal structure of BCL-W added another layer of structural complexity.

Despite sequence identities of less than 25%, structures of other family members are found to be more similar to each other than the three available structures of BCL-W to each other. In these divergent BCL-W structures, the only difference is the length of the construct, which will become important later (see Results).

We reasoned that, to clarify the structural situation and heterogeneity around BCL-W, a crystal structure of the ligand binding-competent conformation of BCL-W is of utmost importance. To capture this particular conformation of BCL-W, we used ribosome-display [38,39] selections to generate DARPins [36] that bind to the groove of BCL-W. Co-crystallization of these DARPins with human BCL-W allowed us to determine two identical high-resolution structures of the compact, ligand binding-competent conformation of BCL-W, which we present here as the first crystal structures of BCL-W in this conformation.

The interactions between the two selected DARPins used for co-crystallization and the BCL-W groove differ. Nonetheless, all of our solved BCL-W crystal structures are practically identical, illustrating that the binding of DARPins used for co-crystallization does not alter the intrinsic structure of BCL-W but merely captures it. The obtained structures reveal that the so-determined conformation of BCL-W and the ligand-free conformation of its closest relative BCL-XL are extremely similar. Thus, through the

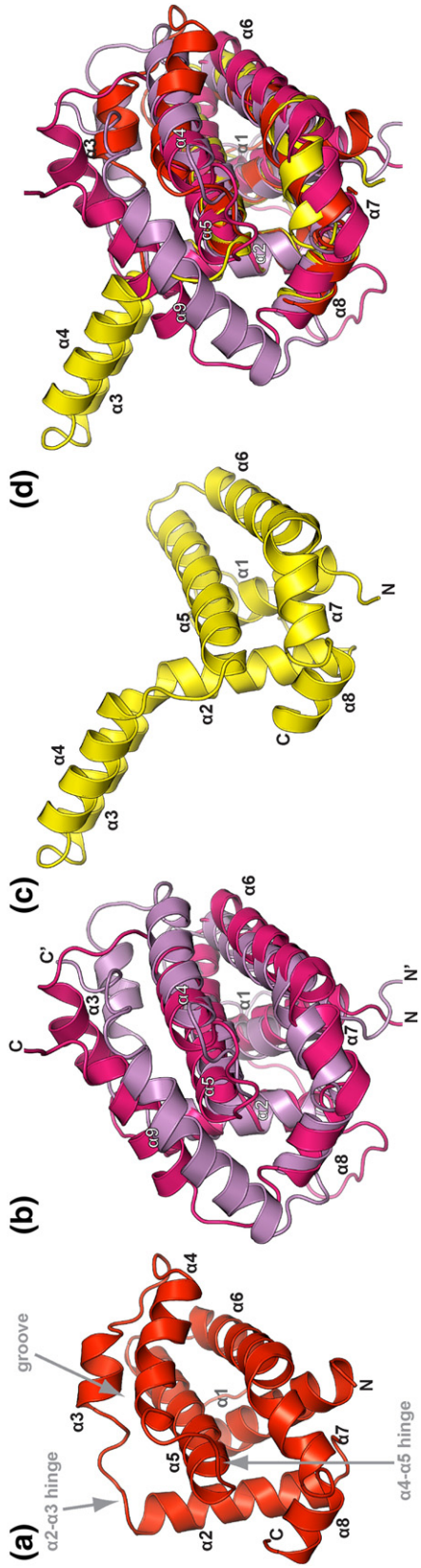

Fig. 1. Structural heterogeneity among the three previously published structures of BCL-W and differences compared to the structure of BCL-XL. Structures are shown as ribbon diagrams. For orientation, BCL-W helices are named. (a) Crystal structure of human BCL-XL (PDB ID: 1MAZ) (red), the first published structure of a BCL-2 family member. (b) Superposition of two BCL-W NMR solution structures PDB ID: 1MK3 (pink) and PDB ID: 1O0L (violet). (c) Domain-swapped BCL-W crystal structure PDB ID: 2Y6W (yellow). (d) Superposition of BCL-XL, both BCL-W NMR structures and the domain-swapped BCL-W crystal structure. Significant deviations exist in the groove, α2-α3 hinge and α4-α5 hinge region between the two NMR structures (pink and violet) and to the BCL-XL structure (red). The first X-ray structure of BCL-W (yellow) shows a large displacement of the important groove formed by α3-α4.

combination of *in vitro* generation of conformation-specific binders, we could co-crystallize the ligand binding-competent conformation of BCL-W, and we present here the first structural explanation for the conformational flexibility of BCL-W.

Results

Crystal structure of the compact, ligand binding-competent BCL-W conformation in complex with groove-binding DARPins

To get access to structures of BCL-W potentially in ligand binding-competent conformations, we used DARPins as a crystallization aid. To select binders interacting with the groove area, and thus to avoid helix α9 of BCL-W to bind itself into this groove, we used a special ribosome-display selection strategy in which all DARPins not binding to the groove region were initially counterselected [36]. To achieve this directing of binders, we preincubated the combinatorial binder library prior to the main selection step with groove-protected BCL-W. Protection of the groove was achieved through complex formation with the BH3-only BIM peptide fused to protein D (pD) of phage lambda. Since the BIM peptide binds into the surface-exposed groove of all BCL-2 family members with high affinity [40], only regions outside of the BCL-W groove area should be accessible to the DARPin library in this initial step. Library members binding outside of the groove region were therefore eliminated upon removal of these complexes [36].

The remaining binders should hence interact with the BCL-W groove region and could be recovered in the following main selection step. Selected binders indeed specifically interacted with the BCL-W groove as determined by competition ELISA experiments with the BIM peptide [36]. The selected binders D12 and H8, which were used for co-crystallization, bound BCL-W with a K_D of 10.3 nM and 643 pM, respectively, as determined by surface-plasmon-resonance measurements [36]. Prior to crystallization trials, complex formation of the binders D12 and H8 with BCL-W was tested by analytical size-exclusion chromatography and compared to the BCL-W/pD-BIM complex formation. As found for the BH3-only pD-BIM peptide ligand, equimolar addition of binder D12 or H8 to BCL-W led to the formation of a 1:1 target:ligand complex (Fig. S2).

Two crystal structures of BCL-W in complex with DARPin D12 and in complex with DARPin H8 were determined. The BCL-W/D12 and the BCL-W/H8 complex structures were solved at a resolution of 1.5 and 1.85 Å, respectively. Crystallographic statistics are summarized in Table ST1. Both selected DARPins bind into the surface-exposed hydrophobic groove of BCL-W via their elongated β-turns in a very similar orientation (Fig. 2). In both the BCL-W/D12 and the BCL-W/H8 structures, the C-terminal helix α9 (residues 167–182, LEEARRLREGNWASVR) of BCL-W that had been found to bind into the groove in both published NMR structures of BCL-W [21,22] is not in the groove and is not resolved. Thus, both selected DARPins displace helix α9 by binding to the surface-exposed groove on BCL-W, thereby mimicking groove-specific interactions of natural, pro-apoptotic BH3-only ligands [21]. A complete list of interactions for both BCL-W/D12 and BCL-W/H8 structures is given in Tables ST2 and ST3, respectively, and they are illustrated in detail in Figs. S3, S4, S5 and S6.

The complex structures show that the BCL-W/DARPin interface is formed by the randomized surface of the DARPin (Fig. 3; for a more detailed illustration, see Figs. S3, S4, S5 and S6), with its β-turns buried inside the hydrophobic groove of BCL-W. The interactions between both DARPins and the BCL-W groove are governed primarily by extensive hydrophobic contacts. Buried, interacting β-turn positions of D12 are characterized by large, aromatic residues, whereas the amino acids at the same positions of H8 possess mainly short, aliphatic side chains. Polar residues of both the β-turn stems and the helical binding interface of the DARPins interact with the polar residues of amphipathic helices α2 and α3 of BCL-W via a network of hydrogen bonds.

A view from the N-terminus of both DARPins along the BCL-W groove in Fig. 3 reveals that, in both cases, a positively charged DARPin residue (DARPin D12: Lys45 and DARPin H8: Arg45) followed by an aromatic amino acid (DARPin D12: Tyr46 and DARPin H8: Phe46) interacts with the α2-α3 hinge of BCL-W. These interactions are followed by a continuous stretch of hydrophobic DARPin β-turn residues interacting with the bottom of the BCL-W groove and are combined with hydrogen bond interactions of both DARPins to the end of the groove formed by the α-hairpin of helices α3 and α4. Interestingly, an extremely similar arrangement of interactions exists for the previously reported BCL-XL/BIM complex crystal structure (PDB ID: 1PQ1) [41] (see below). Together with the observed displacement of helix α9, this illustrates the capacities of the selected DARPin binders to mimic natural α-helical ligands, even though by using adjacent β-turns, and it convincingly demonstrates the efficacy of the applied directed evolution method.

The interaction of H8 with BCL-W (K_D = 643 pM) is much stronger than the interaction of D12 (K_D = 10.3 nM). As the hydrogen bonding pattern of the BCL-W/D12 and BCL-W/H8 interactions is largely similar (Tables ST2 and ST3, as well as Figs. S4, S5 and S6), we assume that the higher affinity of H8 for BCL-W originates from a better fit of the smaller aliphatic amino acids at its β-turn tip with hydrophobic groove residues of BCL-W and from the decreased distance between H8 and BCL-W.

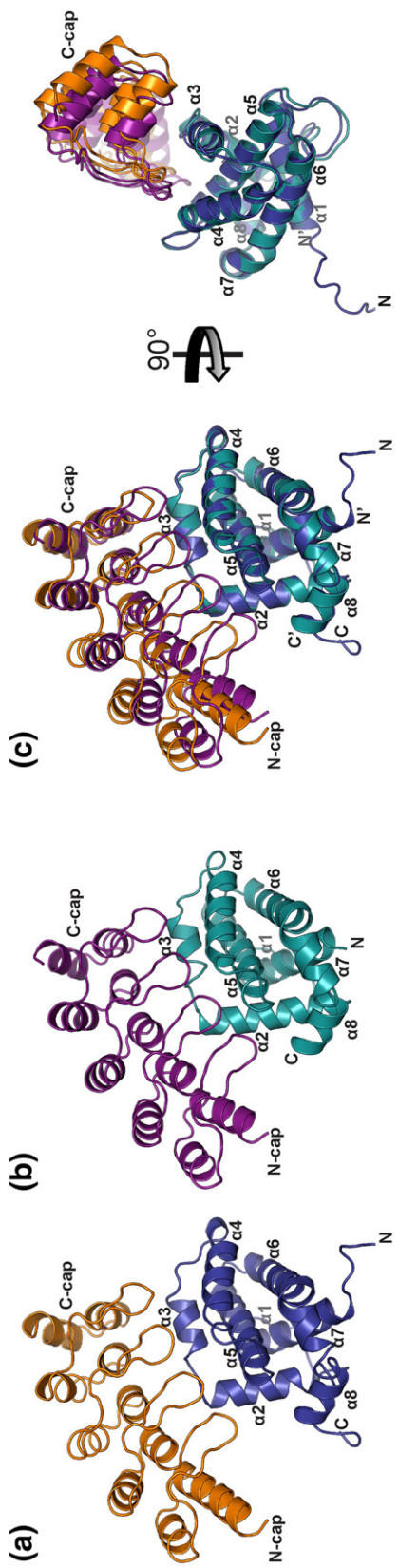

Fig. 2. Crystal structures of the BCL-W/D12 and the BCL-W/H8 complex. Structures are shown as ribbon diagrams. For orientation, positions of the DARPin N- and C-cap, as well as BCL-W helices, are indicated. (a) The 1.5-Å crystal structure of DARPin D12 (orange) in complex with BCL-W (blue). (b) The 1.85-Å crystal structure of DARPin H8 (purple) in complex with BCL-W (cyan). (c) Superposition of the BCL-W/D12 and BCL-W/H8 complex structure. Both selected DARPins bind into the surface-exposed hydrophobic groove of BCL-W via their elongated β-turns in a very similar orientation.

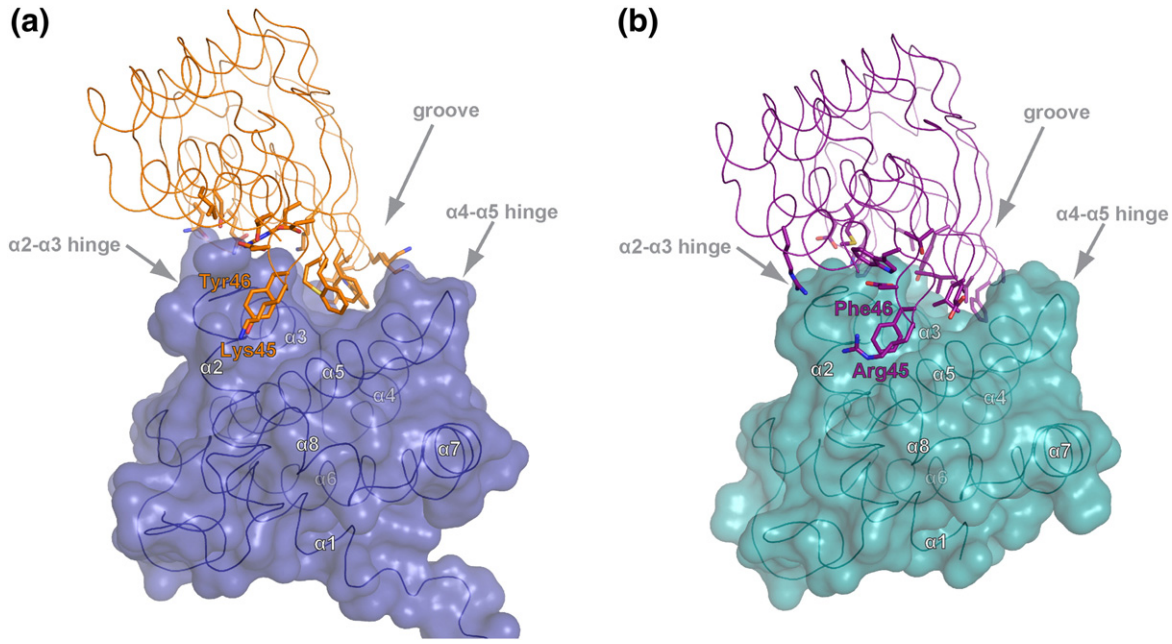

Fig. 3. Binding of DARPins to the BCL-W groove. (a) View along the BCL-W groove in the BCL-W/D12 complex from the N-terminal end of the DARPin. (b) View along the BCL-W groove in the BCL-W/H8 complex. BCL-W is shown as a transparent, molecular surface with a ribbon representation of the protein backbone in blue and cyan. The corresponding DARPins D12 and H8 are shown in orange and purple in a ribbon diagram with interacting amino acid side chains highlighted as sticks. (For details, see Tables ST2 and ST3, where the interactions are tabulated).

Comparison of all available BCL-W surface groove structures

We elucidated how the hinge and groove regions of the new structures in their compact, ligand binding-competent conformation differed from the previous structures of BCL-W.

In total, we solved three BCL-W structures: the BCL-W/D12 complex structure and two BCL-W/H8 complex structures present in the asymmetric unit of crystals from the BCL-W/H8 complex (see Table ST3 and Figs. S5, S6 and S7). Despite the differences in DARPin interactions, the structure of the hinge and groove region is practically identical in all of our BCL-W crystal structures, illustrating that the binding of DARPins used for co-crystallization does not alter the intrinsic structure of BCL-W. Significant deviations in this region are found between our structures and both NMR structures, as well as the domain-swapped X-ray structure. Interestingly, major deviations are also found between both NMR structures. For a detailed analysis, see Fig. S8.

Overall structural comparison of BCL-W_{D12} with other anti-apoptotic BCL-2 family proteins

We also wanted to compare the *overall* architecture of our new structure of BCL-W to other available anti-apoptotic BCL-2 family protein structures (Fig. 4). Previous studies have shown that, despite an overall divergence in amino acid sequence, anti-apoptotic members of the BCL-2 family exhibit a remarkably similar three-dimensional structure [42]. The BCL-W_{D12} structure (blue) was superimposed with (a) the first BCL-W NMR solution structure (BCL-WΔC22; PDB ID: 1MK3) [21] (pink), (b) the second BCL-W NMR solution structure (BCL-WΔC10; PDB ID: 1O0L) [22] (violet), (c) the domain-swapped BCL-W crystal structure (BCL-WΔC29; PDB ID: 2Y6W) [37] (yellow), (d) the BCL-XL crystal structure (PDB ID: 1MAZ) [19] (red), (e) the BCL-2 crystal structure (PDB ID: 2XA0) [43] (green) and (f) the MCL-1 crystal structure (PDB ID: 2PQK) [18] (orange).

Deviations are present in the groove region between all structures of the family. However, the structure outside the groove region is largely identical among all family members. The comparison of the BCL-W_{D12} structure (blue) with the first NMR structure of BCL-W (BCL-WΔC22; PDB ID: 1MK3) (pink) is shown in Fig. 4a. Apart from the presence of helix α9 (binding to the hydrophobic groove in 1MK3), the major difference between the two structures is the displacement of α3 away from the protein core and toward the bound helix α9 in 1MK3. Caused by the displacement of α3, the hinge and groove conformations strongly deviate from the BCL-W_{D12} structure. In the second NMR structure of BCL-W (BCL-WΔC10; PDB ID: 1O0L) (violet) (Fig. 4b), helix α9 also binds to the hydrophobic groove, similar to 1MK3. However, helix α9 of 1O0L is more extended and starts earlier

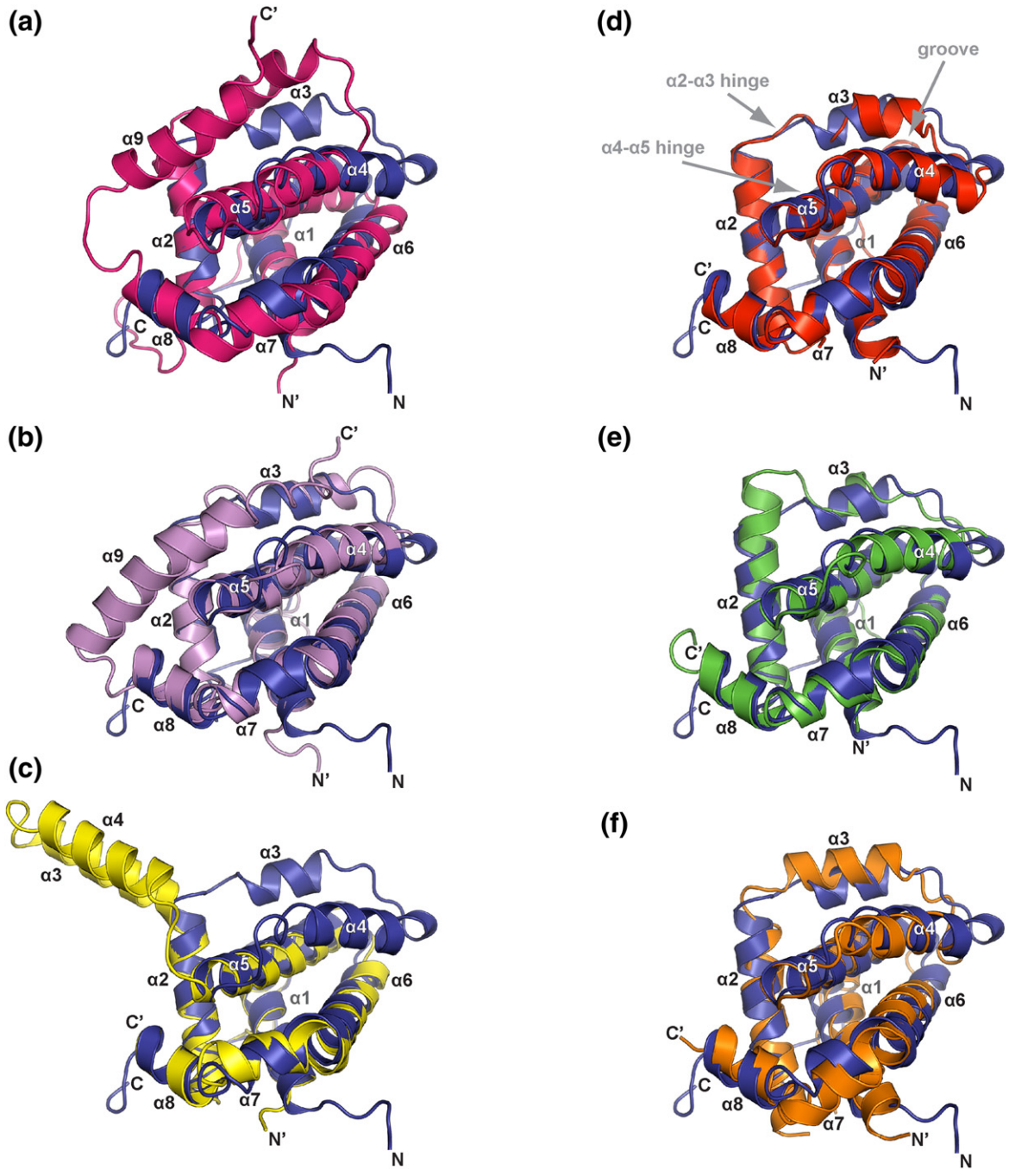

Fig. 4. Overall structural comparison of BCL-W_{D12} with other anti-apoptotic BCL-2 family members. Superposition of BCL-W_{D12} with all available BCL-W structures and with the crystal structures of BCL-XL, BCL-2 and MCL-1. All structures are shown as ribbon diagrams, and α-helices and termini are labeled. Superpositions of BCL-W_{D12} (blue) with (a) the first BCL-W NMR solution structure (BCL-WΔC22; PDB ID: 1MK3) [21] (pink), (b) the second BCL-W NMR solution structure (BCL-WΔC10; PDB ID: 1O0L) [22] (violet), (c) the domain-swapped BCL-W crystal structure (BCL-WΔC29; PDB ID: 2Y6W) [37] (yellow), (d) the BCL-XL crystal structure (PDB ID: 1MAZ) [19] (red), (e) the BCL-2 crystal structure (PDB ID: 2XA0) [43] (green) and (f) the MCL-1 crystal structure (PDB ID: 2PQK) [18] (orange) are shown. Note that 2XA0 [(e) BCL-2] was solved in complex with the BAX BH3-only peptide (data not shown) and 2PQK [(d) MCL-1] was solved in complex with the BIM BH3-only peptide (data not shown).

than that in 1MK3. The displacement of helix α3 seen in 1MK3 is not visible in 1O0L. Altogether, as for 1MK3, the hinge and groove conformations of 1O0L strongly deviate from the BCL-W_{D12} structure.

The superposition of BCL-W_{D12} with the domain-swapped BCL-W crystal structure (BCL-WΔC29; PDB ID: 2Y6W) (yellow) reveals that the structures of helix α1, the α1-α2 loop (not seen from this perspective) and helix α2 are identical up to the C-terminal end of α2 (Fig. 4c). In the BCL-W_{D12} structure, the groove-forming helices α2 and α3 are connected by the well-defined α2-α3 hinge also found in other BCL-2 family proteins (Fig. 4d–f). In contrast, in the 2Y6W structure, the α2-α3 hinge adopts a helical conformation. Thus, α2 is essentially continuous (angle α2 to α3 is nearly 240°, in comparison to an angle of 90° in BCL-W_{D12}) with an elongated shape of α3. Helices α3 and α4 hinge away from the core of the protein. The elongation of α3 and the shortening of the α3-α4 loop results in a closer, almost parallel orientation of α3 and α4. Thus, groove and hinge regions of 2Y6W differ extremely, compared to all other BCL-W structures, including the BCL-W_{D12} structure.

Superposition of BCL-W_{D12} with the BCL-XL crystal structure (PDB ID: 1MAZ) (red) (Fig. 4d) reveals that the compact, ligand binding-competent BCL-W_{D12} conformation is extremely similar to the structure of ligand-free BCL-XL. The only slight deviation between the two structures includes a region stretching from the middle of helix α3 (including the α3-α4 loop) to the N-terminal half of helix α4. In BCL-W_{D12}, this region is horizontally shifted toward the C-terminal end of helix α5 and vertically shifted away from the subjacent helices α5 and α6. The conformation of a large portion of the binding groove itself is practically identical. Importantly, the conformation of both structurally crucial hinge regions (α2-α3 hinge and α4-α5 hinge) is identical (see also the next section). Neither of the previously determined BCL-W structures showed such a high degree of similarity between BCL-W and BCL-XL, which is its closest relative (58% sequence identity).

The superposition of BCL-W_{D12} and the BCL-2 crystal structure (in complex with the BH3 domain of BAX, which is not shown here) (PDB ID: 2XA0) (green) is shown in Fig. 4e. The overall topology of the two proteins is similar. Helix α2 of BCL-2 is extended in comparison to its equivalent in BCL-W_{D12}. The α3-α4 loop possesses an identical conformation in both structures, as do all following structural elements including large parts of the α4-α5 hinge region.

Although MCL-1 marks an outlier from the BCL-2 protein family with regard to its selectivity pattern toward ligands and shares only 25% sequence identity with other family members, its overall three-dimensional structure is again very similar to that of other BCL-2-like proteins, including our structure of BCL-W_{D12}. The structural alignment of the MCL-1 crystal structure (PDB ID: 2PQK) (orange) with BCL-W_{D12} (blue) shown in Fig. 4f reveals that differences are mainly found in the region forming the groove of both proteins. In the MCL-1 structure, the observed outward shift of helices α3 and α4 is caused by a conformational change upon co-crystallization with the BH3-only peptide BIM [18]. As for the BCL-2 structure 2XA0 (Fig. 4e), only the ligand-bound crystal structure of MCL-1 exists.

To summarize, we thus observe striking structural similarities between our solved BCL-W_{D12} structure and other anti-apoptotic BCL-2 family proteins, in particular, the ligand-free structure of the closest relative BCL-XL (PDB ID: 1MAZ) [19]. Thus, we conclude that our described compact, ligand binding-competent conformation of BCL-W represents a physiologically active conformation of BCL-W, which has not been described before in any of the three previously published BCL-W structures.

The BCL-W hinge regions

The α2-α3 and α4-α5 hinge regions form, together with the N-terminal end of helix α5, one end of the surface-exposed groove of anti-apoptotic BCL-2 family members. As the largest deviations between family members and between the previously published BCL-W structures are observed in this region, we investigated this region of BCL-W_{D12} in more detail. In Fig. 5, both hinge regions of BCL-W_{D12} (blue) are compared in (a and d) to: BCL-XL (red); (b and e): the BCL-W NMR structures (pink and violet); (c and f): the domain-swapped BCL-W crystal structure (yellow). Figure 5a–c compare the α2-α3 hinge regions. Figure 5d–f compare the respective α4-α5 hinge regions.

Hinge regions of BCL-W_{D12} (blue) and BCL-XL (red) are completely identical (Fig. 5a and d), whereas large deviations between BCL-W_{D12} and the other BCL-W structures, but also among the other BCL-W structures themselves, can be observed. Residues, which structurally stabilize the hinge regions, are highly conserved between BCL-W and BCL-XL.

Analysis of the α2-α3 hinge shows that the major interactions stabilizing the α2-α3 hinge in BCL-W_{D12} (blue) and BCL-XL (red) are hydrophobic interactions between Phe or Tyr side chains located at the C-terminal end of helix α2, the loop connecting α2 and α3 and the beginning of helix α3 with Ala and Val amino acid side chains at the N-terminal end of helix α5 (Fig. 5a).

However, in the previous BCL-W structures, these interactions are not conserved: only one of these interactions is also found in 1MK3 (pink) and 1O0L (violet), namely the hydrophobic interaction of the Phe side chain located at the C-terminal end of helix α2 with Ala and Val amino acid side chains at the N-terminal end of helix α5 (Fig. 5b). In 1O0L (violet), this interaction is similar to BCL-W_{D12} (blue). In

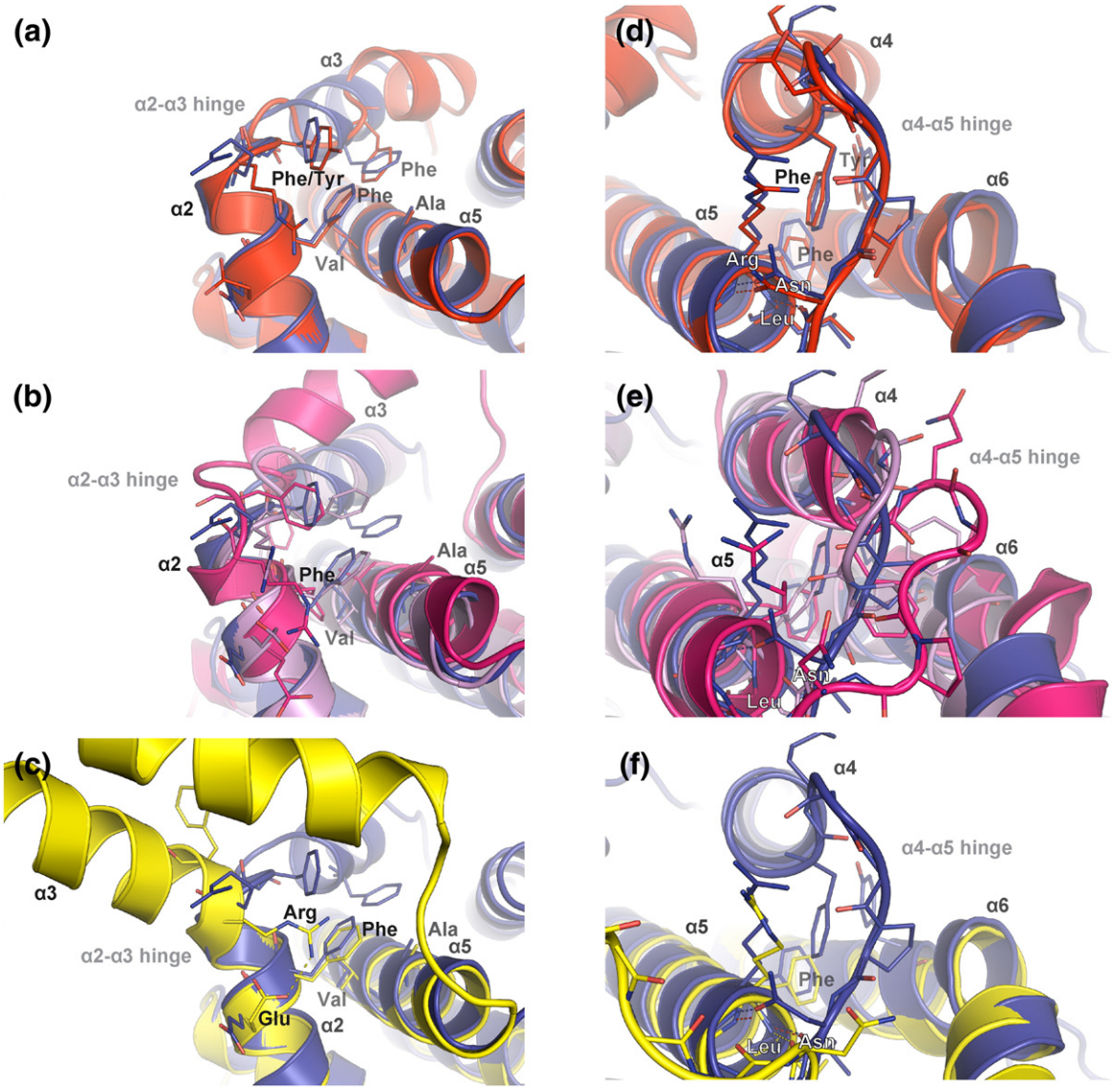

Fig. 5. Investigation of the BCL-W hinge regions. Superposition of the BCL-W_{D12} crystal structure with the crystal structure of BCL-XL and all available BCL-W structures. (a–c) Comparison of the α2-α3 hinge region of BCL-W_{D12} (blue) to the α2-α3 hinge region of (a) the BCL-XL crystal structure (PDB ID: 1MAZ) (red), (b) the BCL-W NMR structures 1MK3 (pink) and 1O0L (violet) and (c) the domain-swapped BCL-W crystal structure 2Y6W (yellow). (d–f) Comparison of the respective α4-α5 hinge regions. Structures are shown in ribbon representation with interacting residues of the hinge region depicted as sticks. Hydrogen bonds are indicated by broken lines and are colored as the respective structures. For sequence information, see Fig. S1.

1MK3 (pink), the Phe side chain adopts a different conformation but still preserves the interaction. For both 1O0L (violet) and 1MK3 (pink), these are the only stabilizing interactions found in the α2-α3 hinge. All other interactions seen in BCL-W_{D12} (blue) and BCL-XL are not present. The same applies for the domain-swapped 2Y6W (yellow) (Fig. 5c). In addition to the single preserved interaction seen in BCL-W_{D12} (blue) and BCL-XL, a hydrogen bond is formed in 2Y6W between a Glu side chain located at the C-terminal end of α2 and an Arg side chain located in the hinge region, which now initiates helix α3. Although not commented on by the authors [37], we hypothesize that this interaction adds to the stabilization of the domain swap.

Like the α2-α3 hinge region, the α4-α5 hinge of BCL-W_{D12} (blue) and that of BCL-XL (red) are completely identical (Fig. 5d). At the beginning of the hinge, a Phe side chain located in the α4-α5 loop is involved in hydrophobic interactions with a Phe

side chain located at the N-terminal end of helix α5 and with a Tyr side chain located at the C-terminal end of helix α6. Two hydrogen bonds, between an Asn side chain and an Arg backbone and between an Asn backbone and a Leu backbone, stabilize the conformation of the hinge end.

Again, in the previously published BCL-W structures, these interactions are not conserved: in 1MK3 (pink), all of these interactions are absent. In 1O0L (violet), the only interaction also seen in BCL-W_{D12} (blue) and BCL-XL is the Asn backbone–Leu backbone hydrogen bond (not visible from this perspective) (Fig. 5e). All other interactions are missing. For 1O0L (violet), this is the only interaction that stabilizes the hinge. The hinge in 1MK3 (pink) is not stabilized at all. Interestingly, the Asn at the end of the hinge is the pivot point, where the domain-swapped 2Y6W (yellow) structure hinges away (Fig. 5f). As in 1O0L, only the Asn backbone–Leu backbone hydrogen bond seen in the BCL-W_{D12} (blue) and BCL-XL is also present in the domain-swapped 2Y6W (yellow). Due to the domain swap, the hydrophobic interaction between the Phe side chain located in the α4-α5 loop and helices α5 and α6 present in BCL-W_{D12} (blue) and BCL-XL is lost as well.

To summarize, in addition to the striking overall structural similarities between our solved BCL-W_{D12} structure and the structures of other anti-apoptotic BCL-2 family proteins, the stabilizing hinge interactions found in our BCL-W_{D12} structure and the (ligand-free) BCL-XL (PDB ID: 1MAZ) [19] structure are completely identical. Based on these observations, we conclude that the conformation of BCL-W presented here is the first crystal structure of BCL-W in its compact, ligand binding-competent conformation and thus a valuable addition to the growing ensemble of structures of the BCL-2 protein family. It should thus allow much more relevant drug design.

Structural basis for the conformational flexibility of the BCL-W groove region

Since stabilizing hinge interactions in our BCL-W_{D12} structure and in the BCL-XL (PDB ID: 1MAZ) [19] structure are completely identical (Fig. 5), we reason that the cause for the conformational flexibility of the BCL-W hinge and groove region cannot originate from the hinge regions but must be located elsewhere in the BCL-W structure. We hypothesize that differences between BCL-W and BCL-XL must be located somewhere in the stabilizing interactions between the groove formed by helices α3 and α4 with the helices α5 and α6 lying below.

Therefore, we investigated the interactions of the α3-α4 helical hairpin with the α5-α6 helical hairpin of BCL-W_{D12} (blue) in more detail and compared these interactions to interactions found in BCL-XL (red) (Fig. 6). Figure 6a shows that residues facilitating interactions between helix α3 and α5 are identical in BCL-XL (red) and BCL-W_{D12} (blue). Starting at the N-terminal end of helix α3, Phe and Ala side chains interact similarly with Phe, Ala and Leu side chains located at helix α5 in BCL-XL (red) and BCL-W_{D12} (blue). The first interacting residue that is not identical between BCL-XL and BCL-W_{D12} causes a major difference in interactions of the α3-α4 loop with helices α5 and α6 (Fig. 6b): in BCL-XL (red), an Ile of the α3-α4 loop completely fills a hydrophobic cavity formed by a Leu from helix α5 and a Leu and Trp from helix α6. In contrast, in BCL-W_{D12} (blue), this α3-α4 loop residue is a Val, which does not fill the hydrophobic cavity, thereby significantly weakening the interaction of the α3-α4 helical hairpin with the α5-α6 helical hairpin of BCL-W_{D12}.

Additional differences between BCL-XL and BCL-W_{D12} are found in interactions between helix α4 and α6 (Fig. 6c). In BCL-XL (red), starting at the N-terminal end of helix α4, a network of hydrophobic interactions keeps helices α4 and α6 together. Major differences can be seen in this area between BCL-XL and BCL-W_{D12}. Side chains in BCL-W_{D12} (blue) are much smaller than in BCL-XL (red), and as a consequence, major interactions found within BCL-XL (red), such as the interactions between a Tyr on helix α4 with a Trp, Thr and Tyr of helix α6, are missing in BCL-W_{D12} (blue). This leaves a large hole between helix α4 and α6 in BCL-W_{D12} (blue).

We conclude that, together with the weakened interaction of the α3-α4 loop with helices α5 and α6 (Fig. 6b), this is a major determinant for the weakened interaction between the α3-α4 helical hairpin and the α5-α6 helical hairpin of BCL-W_{D12}, which accounts for the conformational flexibility seen in the BCL-W groove region. The stabilizing interaction at the transition to the α4-α5 hinge is again identical between BCL-XL (red) and BCL-W_{D12} (blue), where a hydrogen bond between an Asn on helix α4 and a Tyr on helix α6 in BCL-XL (Asp instead of Asn in BCL-W_{D12}) ties the two helices together (Fig. 6c).

In summary, Fig. 6b and c show residues that differ between BCL-XL and BCL-W that *allow* an identical hinge and groove formation but *stabilize* it more in BCL-XL.

Stabilization of the compact, ligand binding-competent BCL-W conformation through helix α9 or ligands

So far, there had been three structures of BCL-W reported, which only differed in the length of the expressed BCL-W construct. The NMR structure of the longest BCL-W construct BCL-WΔC10 was determined by Hinds *et al.* [22] (PDB ID: 1O0L). Denisov *et al.* determined the NMR structure of the shorter BCL-W construct BCL-WΔC22 (1MK3) [21].

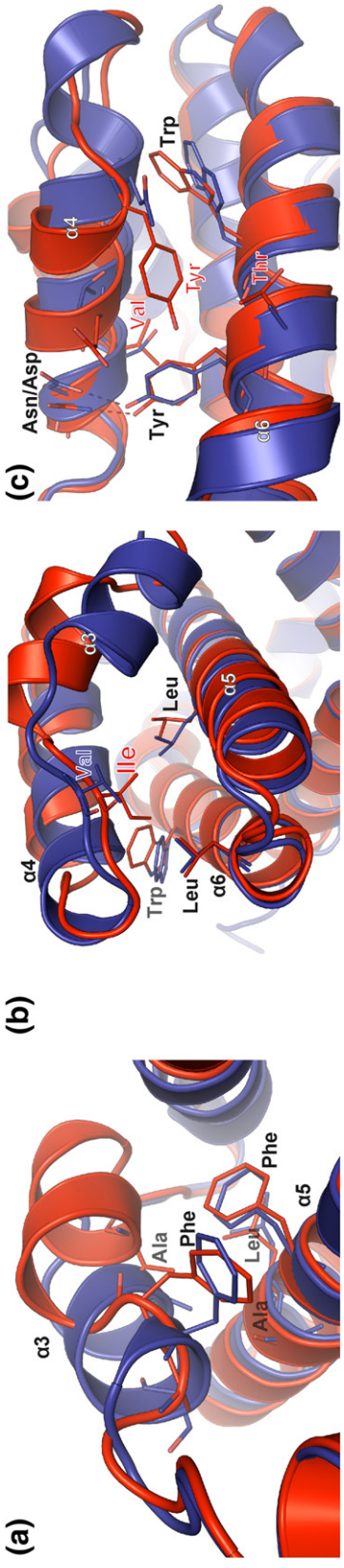

Fig. 6. Interactions of the α3-α4 helical hairpin with the α5-α6 helical hairpin of BCL-W_{D12} (blue) compared to the BCL-XL crystal structure (PDB ID: 1MAZ) (red). (a) Residues facilitating interactions between helix α3 and α5. (b) Interactions of the α3-α4 loop with helices α5 and α6. (c) Interactions between helix α4 and α6. Structures are shown in ribbon representation with interacting residues depicted as sticks. Hydrogen bonds are indicated by broken lines and are colored similar to the respective structures.

The crystal structure of the shortest BCL-W construct BCL-WΔC29 was recently determined by Lee *et al.* [37] (2Y6W). We noticed that shortening of the construct leads to an increase in conformational flexibility in the groove region (Fig. 4). As helix α9 becomes shorter from BCL-WΔC10 (1O0L) (Fig. 4b, violet) to BCL-WΔC22 (1MK3) (Fig. 4a, pink), helix α3 is displaced away from the protein core and toward the bound helix α9 in BCL-WΔC22. Further shortening of helix α9 leads to a complete swap of the entire groove, formed by helices α3 and α4, away from the core of BCL-W in the domain-swapped BCL-WΔC29 (2Y6W) (Fig. 4c, yellow).

Based on extensive structural analyses of all available BCL-W structures, including our determined structures and their comparison to the ligand-free BCL-XL structure, we propose a model, where binding of helix α9, or the DARPin in our case, to the hydrophobic surface-exposed groove of BCL-W stabilizes the hinge regions of BCL-W and serves as a bridge, linking the α2-α3 hinge, helix α3 and helix α4 to the helices α5 and α6. This bridging counterbalances the weak interactions between the α3-α4 helical hairpin and the α5-α6 helical hairpin of BCL-W and thus keeps BCL-W in its compact, ligand binding-competent conformation.

Figure 7a shows that helix α9 of BCL-WΔC22 (1MK3) (pink) makes hydrophobic contacts to the α2-α3 hinge region. Starting at the N-terminal end of helix α9, a Leu and two Arg side chains interact with

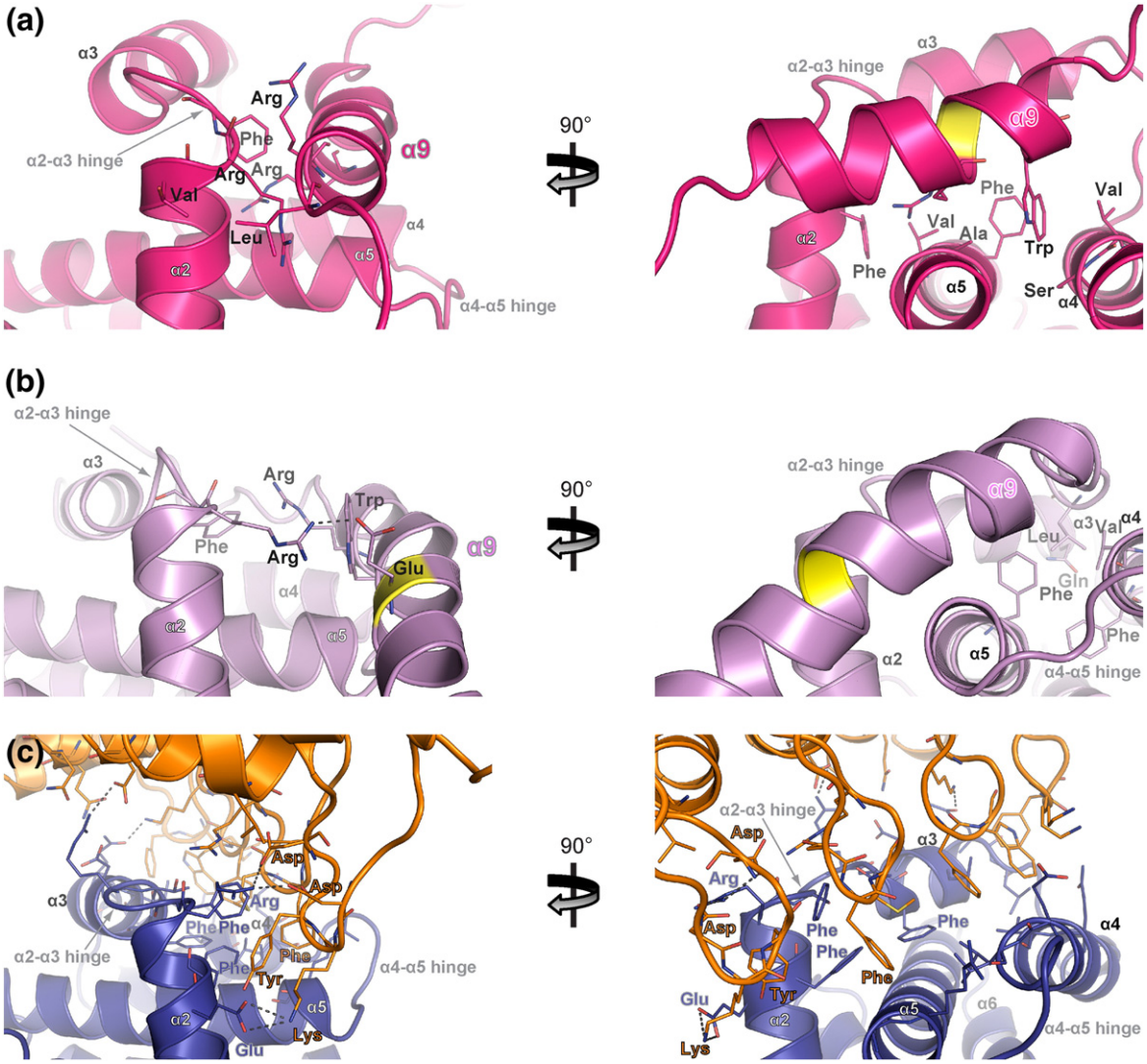

Fig. 7. Stabilization of the compact, ligand binding-competent BCL-W conformation through helix α9 or ligands. Interactions of helix α9 with the hinge and groove region of (a) BCL-WΔC22; PDB ID: 1MK3 (pink) and (b) BCL-WΔC10; PDB ID: 1O0L (violet). (c) Interactions between DARPin D12 (orange) and BCL-W_{D12} (blue). Structures are shown in ribbon representation with interacting residues depicted as sticks. Hydrogen bonds are indicated by black broken lines.

a Phe, Val, Arg and another Phe side chain located in the α2-α3 hinge. Additionally, a Trp side chain located at the C-terminal end of helix α9 fills a hydrophobic cavity formed by a Val and Ser of helix α4 and an Ala, Val and Phe of helix α5. The domain-swapped BCL-WΔC29 construct is seven amino acids shorter than the BCL-WΔC22 construct. To indicate (in the BCL-WΔC22 (1MK3) structure) where the sequence of the domain-swapped BCL-WΔC29 construct would end, the corresponding position is highlighted in yellow (seen better on the right).

Surprisingly, interactions between helix α9 and the hinge and groove region of BCL-WΔC10 (1O0L) (violet) are different (Fig. 7b). A Glu side chain on helix α9 forms a hydrogen bond to an Arg located in the α2-α3 hinge. This interaction is followed by hydrophobic contacts between helix α9 residues Trp and Arg to a Phe side chain of the α2-α3 hinge. The only interaction of the non-helical portion of BCL-WΔC10 that is C-terminal of helix α9 is the hydrophobic interaction of a Leu reaching into a hydrophobic pocket formed by a Gln of helix α3, a Phe and Val of helix α4 and a Phe located in helix α5. Again, the last position of the domain-swapped BCL-WΔC29 construct is highlighted in yellow in the BCL-WΔC10 (1O0L) structure to indicate where the sequence of the domain-swapped construct would end.

Although interactions of helix α9 clearly differ between the two NMR structures (Fig. 7a and b), the complete absence of these interactions obviously influences the BCL-W structure. While the described hydrogen bond between Glu on helix α9 and Arg in the α2-α3 hinge [seen in BCL-WΔC10 (1O0L) (Fig. 7b, violet)] would be possible in the domain-swapped BCL-WΔC29 construct, the remaining interactions and the important cavity-filling Trp, contributed by α9 and mediating the interaction in the BCL-WΔC22 (1MK3) (pink), would be missing. Lee *et al.* did not comment on the absence of these interactions, but their lack may be indeed the major reason for the domain swap of the BCL-WΔC29 construct [37].

Figure 7c shows the complex structure of DARPin D12 binding into the hydrophobic groove of BCL-W_{D12} with all interacting residues highlighted as sticks (see also Fig. S4 and Table ST2). A large number of DARPin D12 residues interact with the BCL-W_{D12} groove over its entire length.

The view from the N-terminus of D12 along the BCL-W_{D12} groove shows the network of hydrogen bonds between the DARPin and the α2-α3 hinge of BCL-W_{D12} at the entrance of the groove. A Lys and two Asp side chains from the DARPin form hydrogen bonds to a Glu and an Arg in helix α2. These two BCL-W side chains formed the stabilizing hydrogen bond in the domain-swapped 2Y6W structure (Fig. 5c). Interestingly, the DARPin separately engages the Glu and Arg side chains in helix α2 of BCL-W_{D12} in the formation of hydrogen bonds, thereby preventing them from forming the stabilizing hydrogen bond found in the domain-swapped 2Y6W structure. Moreover, a Tyr and a Phe from the DARPin interact with hydrophobic Phe side chains located in the α2-α3 hinge of BCL-W_{D12}. These interactions are followed by a continuous stretch of hydrophobic β-turn DARPin residues, which interact extensively with the bottom of the BCL-W groove, formed by helix α5 and with helices α3 and α4. This interaction network is combined with hydrogen bond interactions of the DARPin to the end of the groove, formed by the α-hairpin of helices α3 and α4. As discussed before, a strikingly similar arrangement of interactions also exists in the previously reported BCL-XL/BIM complex crystal structure (PDB ID: 1PQ1) [41] (Fig. S9).

In summary, BCL-W clearly possesses a high degree of conformational flexibility in its groove region and hinge regions. Stabilizing interactions are important for the structural integrity of the BCL-W groove, exemplified by their conserved sequence across family members (Fig. S1). While the stabilizing hinge interactions between our BCL-W_{D12} structure and the BCL-XL (1MAZ) [19] structure are completely identical (Fig. 5), we deduce that the determinants for the conformational flexibility of the BCL-W groove area are not the hinge regions but, rather, the weaker interactions between the α3-α4 helical hairpin and the α5-α6 helical hairpin of BCL-W (Fig. 6).

Both helix α9 and DARPin D12 make contacts to the hinge and groove regions of BCL-W. The more these interactions extend toward the end of the groove formed by the α-hairpin of helices α3 and α4, the less displacement of the groove away from the protein core occurs (Figs. 4 and 7) (degree of displacement: BCL-WΔC29 > BCL-WΔC22 > BCL-WΔC10 > BCL-W_{D12}). Thus, we propose a model in which binding of helix 9, or binding of DARPins in our case, to the hydrophobic surface-exposed groove of BCL-W (i) stabilizes the hinge regions and (ii) serves as a bridge, which links the α2-α3 hinge, helix α3 and helix α4 to the helices α5 and α6. This bridging function compensates for the weak interactions between the α3-α4 helical hairpin and the α5-α6 helical hairpin of BCL-W and thus keeps BCL-W in its compact, ligand binding-competent conformation (Fig. 8).

Discussion

The BCL-W hinge and groove region differ significantly between previously determined BCL-W structures and made this family member quite distinct from its close relatives. However, the underlying structural determinants for this increased conformational flexibility and heterogeneity of BCL-W, contrasted by the high level of structural similarity among the remaining family members (BCL-2, BCL-XL and MCL-1), remained elusive. We selected high-affinity DARPins binding to the groove of BCL-W using ribosome

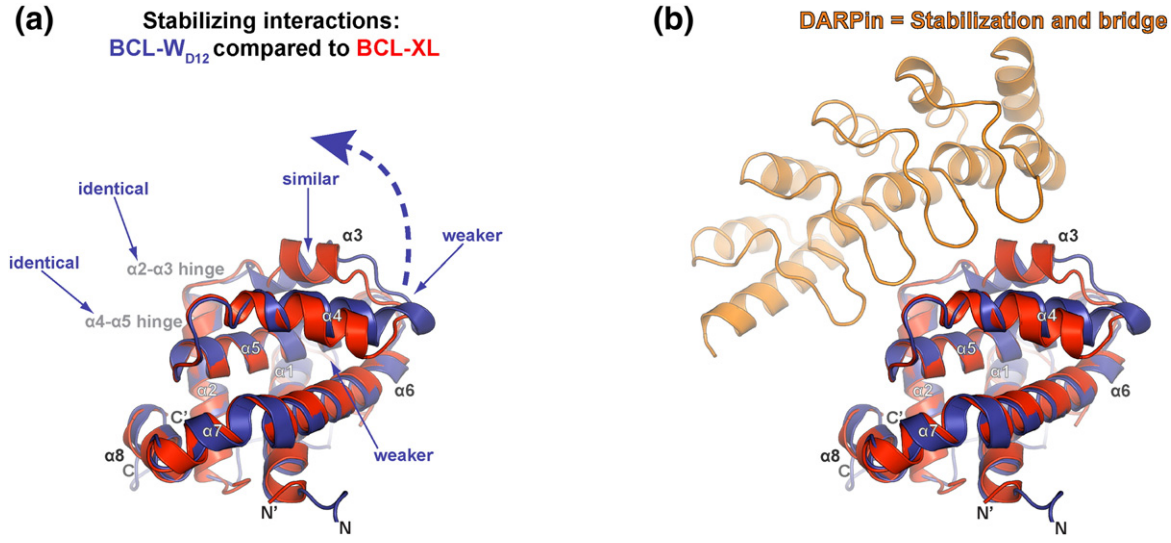

Fig. 8. Model for the stabilization of the compact, ligand binding-competent conformation of BCL-W. Superposition of the BCL-W$_{D12}$ crystal structure with the crystal structure of BCL-XL (PDB ID: 1MAZ). Structures are shown in ribbon representation. (a) Comparison of interactions stabilizing the compact, ligand binding-competent conformation of BCL-W (blue) and BCL-XL (red). Interactions at hinge regions are identical in the two proteins. However, interactions between the α3-α4 helical hairpin and the α5-α6 helical hairpin are weaker in BCL-W. The resulting increased conformational flexibility of the BCL-W groove region and its displacement tendency is indicated by a blue broken arrow. (b) Binding of DARPins (or helix α9) to the hydrophobic surface-exposed groove of BCL-W stabilizes the hinge regions and serves as a bridge linking the α2-α3 hinge, helix α3 and helix α4 to the subjacent helices α5 and α6. This bridging function compensates for the weak interactions between the α3-α4 helical hairpin and the α5-α6 helical hairpin of BCL-W and thus keeps BCL-W in its compact, ligand binding-competent conformation.

display to capture the compact, ligand binding-competent conformation of BCL-W, and we were able to determine the first crystal structures of BCL-W in this conformation. Although the interaction pattern of the DARPins used for co-crystallization differ, all three of our high-resolution BCL-W structures are practically identical, illustrating that the binding of DARPins does not alter the intrinsic structure of BCL-W.

A comparison of our BCL-W crystal structure to the crystal structure of ligand-free BCL-XL, the closest relative of BCL-W within the anti-apoptotic BCL-2 family, reveals for the first time striking similarities in the hinge and groove area of the two proteins. Thus, we deduce that our described conformation of BCL-W represents a physiologically active conformation of BCL-W.

The hinge regions are obviously important for the structural integrity of the groove area, but since we find the hinge conformations of our BCL-W structure and BCL-XL to be completely identical, we suggest that the reason for the increased conformational flexibility of the BCL-W hinge and groove region must be located elsewhere in the BCL-W structure. Indeed, we identified key differences between our BCL-W ligand binding-competent structure and the structure of BCL-XL to be interactions between the α3-α4 helical hairpin and the subjacent α5-α6 helical hairpin. Crucial interactions seen in this area of BCL-XL are missing in BCL-W or are weakened. We thus conclude that this is the major reason for the increased flexibility of the BCL-W groove region.

BCL-W is unique among the anti-apoptotic BCL-2 family members, as it possesses an additional C-terminal helix (α9) in front of its transmembrane helix. Helix α9 can bind to the groove and interact with the hinge region and with side chains along the groove formed by helices α3 and α4 and with the subjacent helix α5. Similar, but more pronounced, these interactions are also formed by our groove-binding DARPins and by the BH3-only BIM peptide in the BIM/BCL-XL complex crystal structure. Through the analysis of the previously published BCL-W structures, we recognized that the stepwise truncation of helix α9 leads to an increased displacement of the groove. On the basis of our data and analyses, we thus propose a model in which helix α9, or the DARPin in our case, keeps BCL-W in its compact, ligand binding-competent conformation. This is achieved through contacts that stabilize the conformation of the hinge region and compensate for the weakened interactions of the α3-α4 helical hairpin with the subjacent α5-α6 helical hairpin.

Since displacement of helix α9 is a prerequisite for the binding of BH3-only peptides, or DARPins in our case, to the surface-exposed BCL-W groove, the conformations of BCL-W, in which helix α9 is bound and displaced, must be interchangeable. Although the question of the physiological importance of the regulation of this conformational flexibility of the BCL-W groove remains to be investigated further, with our crystal structure of BCL-W in its compact,

ligand binding-competent conformation and its analysis, we provide new insights into the structural basis underlying the conformational flexibility of BCL-W. Since crystal structures of the compact, ligand binding-competent conformation of all anti-apoptotic BCL-2 family members have been determined, with the exception of BCL-W, our presented work fills this gap in the structural characterization of the anti-apoptotic BCL-2 protein family. As this family has increasingly attracted the attention of the pharmaceutical industry as important drug targets, the presented BCL-W crystal structure could be highly valuable for future structure-based drug design.

Materials and Methods

Protein production and purification

Generation of coding sequences for BCL-W, BIM and selection of DARPins D12 and H8, as well as the expression and purification of BCL-W, pD_BIM and DARPins D12 and H8 were described previously [36].

Analytical size-exclusion chromatography

Analytical gel filtration was carried out at room temperature on an ÄKTAmicro FPLC system with a Superdex 200 PC 3.2/30 column (GE Healthcare Biosciences, Pittsburg, USA). Runs were performed with TBS_{150} [20 mM Tris–HCl (pH 7.5) and 150 mM NaCl] as running buffer at a flow rate of 60 µl/min. Complex formation of BCL-W with either pD-BIM or DARPin D12 or H8 was analyzed. Free BCL-W and ligands (pD-BIM, D12 or H8), as well as equimolar complexes thereof, were used at a concentration of 10 µM.

Crystallization and data collection

IMAC-purified BCL-W and DARPin D12 or H8 were mixed in an equimolar ratio and separated by preparative size-exclusion chromatography in TBS_{150} (pH 8.0) using an ÄKTAexplorer FPLC system with a Superdex 200 16/60 prep-grade column (GE Healthcare Biosciences, Pittsburg, USA). The fraction corresponding to the 1:1 BCL-W:D12 (or BCL-W:H8) complex was subsequently concentrated to 15 mg/ml. Best-diffracting crystals were obtained by using the sitting-drop vapor diffusion method at 4 °C, in a 384-well crystallization plate. The drops contained 0.2 µl of protein and 0.1 µl of reservoir solution equilibrating with 30 µl reservoir. BCL-W/D12 complex crystals grew in 0.1 M Hepes (pH 8.0), 0.2 M $LiSO_4$ and 25% polyethylene glycol 4000. BCL-W/H8 complex crystallization conditions were 0.1 M citric acid (pH 3.3) and 20% polyethylene glycol 6000. Crystal formation was observed within 1–2 weeks from clear solution. Cryoprotection was achieved by adding glycerol to a final concentration of 10%. Diffraction data were collected at beamline PXI (X06SA) of the Swiss Light Source (Villigen, Switzerland) at a temperature of 90 K (see Table ST1 for data collection and refinement statistics). Data were recorded at 1 Å on a PILATUS 6M detector [44]. Images were processed with XDS [45].

Molecular replacement, model building and refinement

Structures were solved by molecular replacement using PHASER molecular replacement [46] from within the CCP4 package [47]. Solving the BCL-W/DARPin complexes by molecular replacement proved challenging due to the lack of a proper BCL-W search structure. All three available BCL-W structures, both NMR-derived solution structures (PDB ID: 1MK3 and 1O0L) and the recently reported domain-swapped crystal structure (PDB ID: 2Y6W), failed during initial search runs. Therefore, a modified (removal of loops and flexible parts of N- and C-terminal regions) BCL-XL crystal structure (PDB ID: 1MAZ) was used for the finally successful molecular replacement runs. For DARPins in the complex structures, a poly-Ala model of the consensus DARPin structure (PDB ID: 2XEE [48]) was used as a search model.

Model building was carried out by using the program Coot [49]. The structures were refined using PHENIX [50]. The BCL-W/D12 complex structure was refined using anisotropic *B*-factors for all non-hydrogen atoms, occupancy refinement of atoms in alternative conformations and target weight optimization. The refinement protocol for the BCL-W/H8 complex included isotropic *B*-factors for all non-hydrogen atoms, occupancy refinement of atoms in alternative conformations and target weight optimization. For final *R*-factors and R_{free} and additional refinement statistics, see Table ST1. Stereochemical properties were analyzed with MolProbity [51] and WHATCHECK [52]. Structure figures were generated in PyMOL[‡].

Data Bank accession numbers

The atomic coordinates of the BCL-W/D12 and BCL-W/H8 complex structures were deposited in the PDB [53] with PDB ID: 4K5A and PDB ID: 4K5B, respectively.

Acknowledgments

We thank Céline Stutz-Ducommun and Beat Blattmann for help in protein crystallization and the staff of beamline PXIII at the Swiss Light Source for support during data collection. We also thank the members of the Plückthun laboratory for valuable discussions. J. Schilling was supported by a pre-doctoral fellowship of the Forschungskredit of the University of Zurich. This work was supported by European Research Council grant 268621 (NEXT-BINDERS) and the Swiss National Science Foundation grant 3100A_146278/1 (both to A.P.).

Appendix A. Supplementary data

Supplementary data to this article can be found online at http://dx.doi.org/10.1016/j.jmb.2014.04.010.

Received 8 January 2014;
Received in revised form 9 April 2014;
Accepted 11 April 2014
Available online 18 April 2014

Keywords:
apoptosis;
anti-apoptotic BCL-2 family;
BCL-W;
ligand binding-competent conformation;
DARPins

† J. Schilling and J. Schöppe contributed equally to this work.
‡ http://pymol.org/.

References

[1] Green DR, Evan GI. A matter of life and death. Cancer Cell 2002;1:19–30.
[2] Troy CM, Salvesen GS. Caspases on the brain. J Neurosci Res 2002;69:145–50.
[3] Walker LSK, Abbas AK. The enemy within: keeping self-reactive T cells at bay in the periphery. Nat Rev Immunol 2002;2:11–9.
[4] Hengartner MO. The biochemistry of apoptosis. Nature 2000;407:770–6.
[5] Cotter TG. Apoptosis and cancer: the genesis of a research field. Nat Rev Cancer 2009;9:501–7.
[6] Cory S, Adams JM. The Bcl2 family: regulators of the cellular life-or-death switch. Nat Rev Cancer 2002;2:647–56.
[7] Rutledge SE, Chin JW, Schepartz A. A view to a kill: ligands for Bcl-2 family proteins. Curr Opin Chem Biol 2002;6:479–85.
[8] Chipuk JE, Fisher JC, Dillon CP, Kriwacki RW, Kuwana T, Green DR. Mechanism of apoptosis induction by inhibition of the anti-apoptotic BCL-2 proteins. Proc Natl Acad Sci USA 2008;105:20327–32.
[9] Czabotar PE, Lessene G, Strasser A, Adams JM. Control of apoptosis by the BCL-2 protein family: implications for physiology and therapy. Nat Rev Mol Cell Biol 2014;15:49–63.
[10] Letai A, Bassik MC, Walensky LD, Sorcinelli MD, Weiler S, Korsmeyer SJ. Distinct BH3 domains either sensitize or activate mitochondrial apoptosis, serving as prototype cancer therapeutics. Cancer Cell 2002;2:183–92.
[11] Voutsadakis IA. Apoptosis and the pathogenesis of lymphoma. Acta Oncol 2000;39:151–6.
[12] Bairey O, Zimra Y, Shaklai M, Okon E, Rabizadeh E. Bcl-2, Bcl-X, Bax, and Bak expression in short- and long-lived patients with diffuse large B-cell lymphomas. Clin Cancer Res 1999;5:2860–6.
[13] Jäger R, Herzer U, Schenkel J, Weiher H. Overexpression of Bcl-2 inhibits alveolar cell apoptosis during involution and accelerates c-myc-induced tumorigenesis of the mammary gland in transgenic mice. Oncogene 1997;15:1787–95.
[14] Jäättelä M. Escaping cell death: survival proteins in cancer. Exp Cell Res 1999;248:30–43.
[15] Wilson JW, Nostro MC, Balzi M, Faraoni P, Cianchi F, Becciolini A, et al. Bcl-w expression in colorectal adenocarcinoma. Br J Cancer 2000;82:178–85.
[16] Shigemasa K, Katoh O, Shiroyama Y, Mihara S, Mukai K, Nagai N, et al. Increased MCL-1 expression is associated with poor prognosis in ovarian carcinomas. Jpn J Cancer Res 2002;93:542–50.
[17] Zhang B, Gojo I, Fenton RG. Myeloid cell factor-1 is a critical survival factor for multiple myeloma. Blood 2002;99:1885–93.
[18] Fire E, Gullá SV, Grant RA, Keating AE. Mcl-1-Bim complexes accommodate surprising point mutations via minor structural changes. Protein Sci 2010;19:507–19.
[19] Muchmore SW, Sattler M, Liang H, Meadows RP, Harlan JE, Yoon HS, et al. X-ray and NMR structure of human Bcl-xL, an inhibitor of programmed cell death. Nature 1996;381:335–41.
[20] Huang Q, Petros AM, Virgin HW, Fesik SW, Olejniczak ET. Solution structure of a Bcl-2 homolog from Kaposi sarcoma virus. Proc Natl Acad Sci USA 2002;99:3428–33.
[21] Denisov AY, Madiraju MSR, Chen G, Khadir A, Beauparlant P, Attardo G, et al. Solution structure of human BCL-w: modulation of ligand binding by the C-terminal helix. J Biol Chem 2003;278:21124–8.
[22] Hinds MG, Lackmann M, Skea GL, Harrison PJ, Huang DCS, Day CL. The structure of Bcl-w reveals a role for the C-terminal residues in modulating biological activity. EMBO J 2003;22:1497–507.
[23] Day CL, Chen L, Richardson SJ, Harrison PJ, Huang DCS, Hinds MG. Solution structure of prosurvival Mcl-1 and characterization of its binding by proapoptotic BH3-only ligands. J Biol Chem 2005;280:4738–44.
[24] Sattler M, Liang H, Nettesheim D, Meadows RP, Harlan JE, Eberstadt M, et al. Structure of Bcl-xL-Bak peptide complex: recognition between regulators of apoptosis. Science 1997;275:983–6.
[25] Liang H, Fesik SW. Three-dimensional structures of proteins involved in programmed cell death. J Mol Biol 1997;274:291–302.
[26] Kutzki O, Park HS, Ernst JT, Orner BP, Yin H, Hamilton AD. Development of a potent Bcl-x(L) antagonist based on alpha-helix mimicry. J Am Chem Soc 2002;124:11838–9.
[27] Tzung SP, Kim KM, Basañez G, Giedt CD, Simon J, Zimmerberg J, et al. Antimycin A mimics a cell-death-inducing Bcl-2 homology domain 3. Nat Cell Biol 2001;3:183–91.
[28] Becattini B, Kitada S, Leone M, Monosov E, Chandler S, Zhai D, et al. Rational design and real time, in-cell detection of the proapoptotic activity of a novel compound targeting Bcl-X(L). Chem Biol 2004;11:389–95.
[29] Kitada S, Leone M, Sareth S, Zhai D, Reed JC, Pellecchia M. Discovery, characterization, and structure-activity relationships studies of proapoptotic polyphenols targeting B-cell lymphocyte/leukemia-2 proteins. J Med Chem 2003;46:4259–64.
[30] Wang JL, Liu D, Zhang ZJ, Shan S, Han X, Srinivasula SM, et al. Structure-based discovery of an organic compound that binds Bcl-2 protein and induces apoptosis of tumor cells. Proc Natl Acad Sci USA 2000;97:7124–9.
[31] Degterev A, Lugovskoy A, Cardone M, Mulley B, Wagner G, Mitchison T, et al. Identification of small-molecule inhibitors of interaction between the BH3 domain and Bcl-xL. Nat Cell Biol 2001;3:173–82.
[32] Enyedy IJ, Ling Y, Nacro K, Tomita Y, Wu X, Cao Y, et al. Discovery of small-molecule inhibitors of Bcl-2 through structure-based computer screening. J Med Chem 2001;44:4313–24.
[33] Walensky LD, Kung AL, Escher I, Malia TJ, Barbuto S, Wright RD, et al. Activation of apoptosis *in vivo* by a hydrocarbon-stapled BH3 helix. Science 2004;305:1466–70.
[34] Baell JB, Huang DCS. Prospects for targeting the Bcl-2 family of proteins to develop novel cytotoxic drugs. Biochem Pharmacol 2002;64:851–63.

[35] Oltersdorf T, Elmore SW, Shoemaker AR, Armstrong RC, Augeri DJ, Belli BA, et al. An inhibitor of Bcl-2 family proteins induces regression of solid tumours. Nature 2005;435:677–81.
[36] Schilling J, Schöppe J, Plückthun A. From DARPins to LoopDARPins: novel LoopDARPin design allows the selection of low picomolar binders in a single round of ribosome display. J Mol Biol 2013;426:691–721.
[37] Lee EF, Dewson G, Smith BJ, Evangelista M, Pettikiriarachchi A, Dogovski C, et al. Crystal structure of a BCL-W domain-swapped dimer: implications for the function of BCL-2 family proteins. Structure 2011;19:1467–76.
[38] Hanes J, Plückthun A. *In vitro* selection and evolution of functional proteins by using ribosome display. Proc Natl Acad Sci USA 1997;94:4937–42.
[39] Zahnd C, Amstutz P, Plückthun A. Ribosome display: selecting and evolving proteins *in vitro* that specifically bind to a target. Nat Methods 2007;4:269–79.
[40] Chen L, Willis SN, Wei A, Smith BJ, Fletcher JI, Hinds MG, et al. Differential targeting of prosurvival Bcl-2 proteins by their BH3-only ligands allows complementary apoptotic function. Mol Cell 2005;17:393–403.
[41] Liu X, Dai S, Zhu Y, Marrack P, Kappler JW. The structure of a Bcl-xL/Bim fragment complex: implications for Bim function. Immunity 2003;19:341–52.
[42] Petros AM, Olejniczak ET, Fesik SW. Structural biology of the Bcl-2 family of proteins. Biochim Biophys Acta 2004;1644: 83–94.
[43] Ku B, Liang C, Jung JU, Oh B-H. Evidence that inhibition of BAX activation by BCL-2 involves its tight and preferential interaction with the BH3 domain of BAX. Cell Res 2011;21: 627–41.
[44] Broennimann C, Eikenberry EF, Henrich B, Horisberger R, Huelsen G, Pohl E, et al. The PILATUS 1M detector. J Synchrotron Radiat 2006;13:120–30.
[45] Kabsch W. XDS. Acta Crystallogr Sect D Biol Crystallogr 2010;66:125–32.
[46] McCoy AJ, Grosse-Kunstleve RW, Adams PD, Winn MD, Storoni LC, Read RJ. Phaser crystallographic software. J Appl Crystallogr 2007;40:658–74.
[47] Collaborative Computational Project, Number 4. The CCP4 suite: programs for protein crystallography. Acta Crystallogr Sect D Biol Crystallogr 1994;50:760–3.
[48] Kramer MA, Wetzel SK, Plückthun A, Mittl PRE, Grütter MG. Structural determinants for improved stability of designed ankyrin repeat proteins with a redesigned C-capping module. J Mol Biol 2010;404:381–91.
[49] Emsley P, Lohkamp B, Scott WG, Cowtan K. Features and development of Coot. Acta Crystallogr Sect D Biol Crystallogr 2010;66:486–501.
[50] Adams PD, Afonine PV, Bunkóczi G, Chen VB, Davis IW, Echols N, et al. PHENIX: a comprehensive Python-based system for macromolecular structure solution. Acta Crystallogr Sect D Biol Crystallogr 2010;66:213–21.
[51] Davis IW, Leaver-Fay A, Chen VB, Block JN, Kapral GJ, Wang X, et al. MolProbity: all-atom contacts and structure validation for proteins and nucleic acids. Nucleic Acids Res 2007;35:W375–83.
[52] Hooft RW, Vriend G, Sander C, Abola EE. Errors in protein structures. Nature 1996;381:272.
[53] Berman HM, Battistuz T, Bhat TN, Bluhm WF, Bourne PE, Burkhardt K, et al. The Protein Data Bank. Acta Crystallogr Sect D Biol Crystallogr 2002;58:899–907.